Novel Zirconium−Titanium Phosphates Mesoporous Materials for Hydrogen Production by Photoinduced Water Splitting

Mahendra P. Kapoor,[§] Shinji Inagaki,* and Hisao Yoshida[†]

Toyota Central R&D Laboratories, Inc., Nagakute, Aichi 480-1192, Japan, and Division of Environmental Research/EcoTopia Science Institute, Nagoya University, Furo-cho, Chikusa, Nagoya 464-8603, Japan

Received: November 1, 2004; In Final Form: February 15, 2005

Syntheses of mesoporous zirconium−titanium phosphates (ZTP) are described under a wide range of synthetic parameters. The ZTP materials showed ordered mesophases whose pore walls are either amorphous or show a lack of correspondence between the structures of adjacent pores. However, the materials showed the reasonable thermal and hydrothermal stability, high specific surface areas, narrow pore size distribution, and considerable pore volumes in the mesophases range. UV−visible and XANES results confirmed the presence of tetrahedrally coordinated zirconium and titanium in the mesoporous framework. ^{31}P NMR measurements provide the details on the coordination structure of Ti, Zr, O, and P connectivities in the mesoporous frameworks. Finally, the ZTP materials demonstrated the considerable activity in photocatalytic decomposition of water for hydrogen generation.

1. Introduction

Several approaches for the fabrication of large surface areas of structured phosphates materials with feature sizes in the nanometer range have been undertaken in the last few decades. Beginning from the crystalline lamellar metal phosphates used in the synthesis of pillared layered structures[1,2] and microporous aluminophosphates with open framework structures,[3] the subsequent work was extended to the compositional range of surfactant-assisted synthesis of mesoporous aluminophosphates.[4] Recently, the synthesis of mesoporous transition metal phosphates gained much attention due to their various applications in nanotechnology. The synthesis of titanium-containing mesoporous aluminophosphates was also attempted with the purpose of obtaining selective oxidation catalysts.[5] Another strategy was the posttreatment or using surfactant with phosphate headgroups for the creation of larger surface area of titanium and zirconium oxide structured surfaces.[6,7] Syntheses of mesoporous vanadium phosphorus oxides were also attempted but material suffered from collapse of regular pore structure during the template removal.[8] Moreover, different research groups published several reports regarding the syntheses of mesoporous zirconium phosphates.[9] Jones et al.[10] used phosphoric acid directly at the stage of the formation of the inorganic matrix along with cetyltrimethylammonium bromide (C_{16}TMABr) as a structure-directing agent (SDA). In other work, the synthesis of high surface area porous zirconium phosphates with uniform pore dimensions and acidic properties was demonstrated with the detailed synthesis procedure using cationic, anionic, or neutral surfactants and the influence of different phosphorus-containing precipitating reagents was also explored.[11] The syntheses of mesoporous titanium phosphate with ion exchange properties, employing cationic and anionic SDAs, were also revealed in the subsequent reports. These materials are described to have a great potential to be used as catalysts for liquid-phase oxidation reactions and light-driven photocatalysis.[12] Also, the proton conductivity of mesoporous zirconium and titanium phosphates was recently described by using impedance spectroscopy.[13]

Usually in a bimetallic system, the influences of one type of metallic species on another are very complex in nature and result in unusual properties, both physical and chemical. Also the preparation of a long life ammonium ion potentiometric membrane sensor based on zirconium titanium phosphate ion exchangers was described.[14] Thus, the possibility to obtain such material with mesoporous texture is very interesting. In this regard, stability, high melting point, low thermal conductivity, high corrosion resistance, and amphoteric behavior are among the improved properties, which recommends that materials could be useful as a catalyst or catalyst support in a number of applications.

In the present article, we describe the synthesis of mesoporous zirconium−titanium mixed phosphates (ZTP) with a range of composition, high surface area, and mesoporous texture. Also, we discuss the synergic effect of zirconium on titanium in the mixed titanium−zirconium mesoporous phosphates, supported by the detailed structural characterization results by XRD, UV−vis, FTIR, ^{31}P MAS NMR, SEM, DTA/TGA, XANES, thermal and hydrothermal stability, and water vapor adsorption measurement. An attempt is also made to describe the possible Ti-, Zr-, P-, and O-connectivities in the mesoporous framework. Finally, the photocatalytic decomposition of water for the hydrogen generation without using any sacrificial agent is also discussed as a potential application.

2. Experimental Section

Materials. Titanium isopropoxide (Wako chemicals) and zirconium *n*-propoxide (70 wt % solution in 1-propanol; Aldrich) were used as Ti and Zr precursors, respectively. Phosphoric acid (H_3PO_4; Wako chemicals) was used as precipitating agent. The octadecyltrimethylammonium chloride (C_{18}TMACl, Tokyo chemi-

* Address correspondence to this author at Toyota Central R&D Laboratories, Inc. Fax: 81-561-636507. Phone: 81-561-638493. E-mail: inagaki@mosk.tytlabs.co.jp.

[§] Present address: Taiyo Kagaku, 1-3 Takaramachi, Yokkaichi, Mie 510-0844, Japan.

[†] Nagoya University.

10.1021/jp045012b CCC: $30.25
Published on Web 04/22/2005

cals) was used as surfactant to synthesize the ZTP materials. A solution of 2 M HCl in ethanol was used for removing the surfactant by the extraction method. Liquid ammonia (25 wt % aq NH_4OH) was used to adjust the pH where necessary. H_2PtCl_6 (Wako chemicals) was used for Pt loading for the catalysis.

Synthesis Procedure. In a typical synthesis of mesoporous zirconium−titanium phosphates (ZTP) with cationic surfactant, the C_{18}TMACl was first dissolved in deionized water (90 g, 5 mol) by heating at 50−60 °C. Zirconium precursor was then added followed by a dropwise addition of H_3PO_4. The gel immediately formed was homogenized by vigorous stirring for 30 min. Titanium isopropoxide dissolved in 2-propanol (w/w) was added very slowly and the pH of the gel was adjusted to 6.5 after 1 h of stirring. Finally, the gel was stirred at room temperature for 3 days. Mixed phosphates with a range of molar compositions were synthesized. The initial molar composition of gels was $[ZrO_2(0-100)/TiO_2(100-0)](1.0):[H_3PO_4](1-4):[C_{18}TMA](1-4):[H_2O](400):[NH_4OH](0.01-0.25)$. The product was filtered off, washed with deionized water, and dried under vacuum at room temperature. Surfactants were then removed by extracting samples with HCl/ethanol solution (2 mL of 2.0 mol % HCl in 150 mL of ethanol) at room temperature for 12 h. For instance, to achieve the higher mesoscopic order the materials with varied Ti/Zr, P/ZrTi, and P/Surfactant molar ratios were also prepared. A similar procedure was adopted for the mesoporous titanium phosphate synthesis, while in the case of mesoporous zirconium phosphate synthesis the pH of the gel was not adjusted during the synthesis.

Characterization. The formation of mesostructure was confirmed with powder X-ray diffraction (PXRD) patterns recorded with a Rigaku RINT-2200 diffractometer with Cu Ka radiation (40 Kv, 30 mA). Nitrogen adsorption−desorption isotherms were obtained with a Quantachrome Autosorb-1 at 77 K and used for BET surface area measurement, pore volume, and pore size distribution calculations. H_2O vapor adsorption−desorption isotherms were recoded on a Belsorp-18 automatic water vapor adsorption apparatus.

UV−visible diffuse reflectance spectra were recorded in the range of 600 to 200 nm under better resolution. FT-IR spectra were performed with a Nicolet FT-IR spectrometer. A scanning electron micrograph (SEM) was taken with a JEOL JSM-890. Transmission electron micrograph (TEM) images were obtained with a JEOL JEM-200CX at an accelerating voltage of 200 kV. A Bruker MSL-300 WB spectrometer was used for ^{31}P MAS NMR at 121.49 MHz and chemical shifts were referenced to H_3PO_4 at 0 ppm.

X-ray absorption near-edge structures (XANES) were obtained in a transmission mode at EXAFS facilities installed on BL-7C of the Photon Factory (KEK, Tsukuba, Japan) with a ring energy of 2.5 GeV and a storage positron current of 180−260 mA with a double-crystal Si (111) monochromator. The higher harmonics were removed by reflecting X-rays on a flat quartz plate at a reflection angle of 5.5 mRad.

Ion-Exchange Capacities. Ion-exchange capacities of the ZTP mesoporous materials were determined by using aqueous solutions of sodium chloride (NaCl, 2 M). About 0.1 g of solid was added to 20 g of NaCl aqueous solution. The resulting suspension was stirred at room temperature for 24 h to reach the equilibrium and thereafter it was titrated potentiometrically by dropwise addition of 0.1 M NaOH (aq).

Photocatalysis. An aqueous solution of H_2PtCl_6 was used for Pt loading by impregnation with use of a rotary vapor under pressure at 60 °C. After drying the samples were reduced in situ photocatalytically [15] or at 300 °C for 3 h in 10% N_2/H_2 flow. Sodium carbonate was used as a pH adjuster as necessary for hydrogen generation as well as for the stability of the photocatalytic reaction system. No sacrificial reagent was used. Typically, 75 mL of water, 2 g of Na_2CO_3 and 0.5 g of Pt loaded ZTP mesoporous catalyst were mixed in a photoreactor cell and irradiated under UV−vis light (>290 nm; 300 W xenon lamp) for a span of reaction times. H_2 production along with O_2 was monitored during the reaction with an online GC system equipped with TCD.

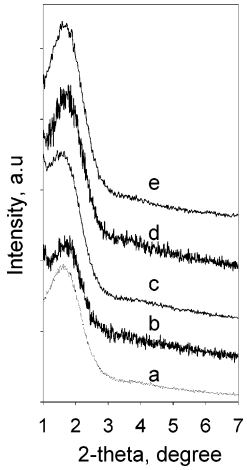

Figure 1. X-ray diffraction patterns of surfactant free zirconium−titanium phosphate (ZTP) materials: (a) $Ti_{100}P$, (b) $Zr_{25}Ti_{75}P$, (c) $Zr_{50}Ti_{50}P$, (d) $Zr_{75}Ti_{25}P$, and (e) $Zr_{100}P$,

3. Results and Discussion

The main advantage is that mixed mesoporous phosphates can be synthesized at room temperature. Since the different preparation parameters usually have an influence on the texture of the mesoporous materials, the variation of zirconium to titanium (Zr/Ti) ratio, precipitating agent, and surfactant concentration (P/S ratio), drying and extraction conditions in the synthesis of ZTP mesoporous material are also very important to have a complete understanding of the related chemistry of the formation of mesoporous ZTP materials. The details on the effects of the described parameters are discussed here.

Powder X-ray Diffraction Analysis. The PXRD patterns of the ZTP materials synthesized according to the procedures described in the Experimental Section showed a single, broad, low-angle diffraction peak. There were no distinctive higher order Bragg reflections (high-angle peaks) that clearly suggest that ZTP are somewhat lower ordered mesophases whose pore walls are amorphous or a lack of correspondence between the structures to adjacent pores. The PXRD patterns of surfactant free mesoporous ZTP materials with a range of compositions are presented in Figure 1. The best results could be obtained when the phosphorus to titanium−zirconium ratio (P/ZrTi) and the phosphorus to surfactant ratio (P/S) were near 2. In all cases, *d*-spacings remained nearly the same before and after removal of the surfactant, whereas the intensities were higher and diffraction patterns were relatively sharp. The TEM image of mesoporous ZTP material (not shown) also revealed the lower ordering of the hexagonal arrangement of mesophases and confirmed that the long-range ordering was absent in mesoporous ZTP materials.

Nitrogen Physisorption. The textural properties of mesoporous ZTP materials with various compositions are compiled

TABLE 1: The Textural Properties of ZTP Mesoporous Materials

sample entery[a]	BET, m^2/g	pore diameter, Å	pore vol, cm^3/g
$T_{100}P$	345	26	0.205
$Z_{25}T_{75}P$	534	25	0.542
$Z_{50}T_{50}P$	570	19	0.583
$Z_{75}T_{25}P$	573	23	0.604
$Z_{100}P$	613	22	0.528

[a] In Z_xT_yP the *x* and *y* indicate the mol % of Zr and Ti, respectively; P/ZrTi = 2.

in Table 1. The materials exhibited nitrogen adsorption−desorption isotherm near type IV. The desorption branch of the isotherm exhibited a different shape of hysteresis depending upon the synthesis parameters and ZTP compositions. BET surface areas of mesopoorus ZTP materials are in the varied range and increased with an increase of zirconium content in the titanium phosphate mesoporous solids (see Table 1). However, the calculated Barrett−Joyner−Halenda (BJH) pore size distribution (from adsorption branch) does not show a consistent variation in pore size with varying compositions. The pore size distribution profiles of ZTP mesoporous solids showed the pore diameters are in a range of 19−26 Å, somewhat lower than those of mesoporous silica prepared with the same surfactants.[16,17] The isotherm shapes and pore size distribution profiles are presented in Figure 2.

Water Vapor Sorption. The water vapor adsorption/desorption isotherm for selected $Zr_{50}Ti_{50}P$ solid was a type-IV and showed a capillary condensation for the mesophase and hysteresis together with a high level of water vapor adsorption at low P/P_o (Figure 3). Due to the adsorption of water vapor at low pressure high level strong interactions between water and the solid surface are very likely and indicate that similar to the titanium phosphate mesoporous materials[12] a charge can be generated and also the exchangeable sites are available in the ZTP mesoporous materials. Similar type-IV isotherms of water adsorption at very low P/P_o were reported for aluminosilcates, and such a phenomenon was correlated to the very strong adsorption of water at the aluminum sites[18,19] whereas in the case of siliceous mesoporous materials, the type-V isotherm was observed.[20−21]

Scanning Electron Microscopy. The SEM micrograph of the $Zr_{50}Ti_{50}P$ mesoporous solid (Figure 4) reveals that tiny crystals of various shapes form aggregates of 0.1 to 0.2 μm. The particles were as small as 50 nm and were almost the same size. And the materials with smaller particles are usually preferable for the potential catalytic applications.

UV−Visible Spectral Analysis. The UV−visible spectra of mesoporous ZTP materials are deconvoluted into two separate peaks (Figure 5) and peak positions with their relative contribution are listed in Table 2. Peak 1 at shorter wavelength (abs 220−235 nm) is assigned to tetrahedral coordination of both titanium and zirconium in the framework, while the longer wavelength peak 2 (abs >290 nm) is typical of the titanium and zirconium present in the extraframework of the material (i.e. five and six coordinated). Titanium phosphate ($Ti_{100}P$) showed the broad absorption spectra in the 210−350 nm wavelength regions whose intensity is mainly due to the electronic transition from O^{2-} (2p) to Ti^{4+} (3d) orbitals. Compared to mesoporous $Ti_{100}P$, the adsorption peak for the mesoporous zirconium phosphate ($Zr_{100}P$) was sharp and assignable to the Zr−O−P coordination. Interestingly, with increasing zirconium content in mesoporous ZTP materials, the absorption peak maximum was shifted to the shorter wavelength region and the intensity of deconvoluted peak 2 was also decreased. Usually in microporous titanium silicates (TS-1) where titanium content is quite low (∼2 mol %) and material have mostly the tetrahedral framework titanium, the strong absorption band at 200−220 nm could be observed due to Ti−O−Si coordination. Thus, the surrounding environment around titanium is also important, whereas in the mesoporous ZTP solids the absorption due to phosphate groups is very crucial. The titanium content is considerably higher in mesoporous ZTP solids that leads to a considerable shift of UV−visible absorption to a longer wavelength.[22] In addition, the phosphate groups are believed to be complexed with the metal oxopolymers and to interact with the positively charged headgroups of the surfactants leading to the complete cross-linking and preventing the ordering of the framework. However, from the observation of UV−visible spectra, it is clear that the presence of zirconium also strongly affects the local structure of titanium in a favorable manner and helps titanium to be present in a tetrahedral coordination.

Infrared Spectroscopy (FTIR). Broad bands in the hydroxyl region (3600−3200 cm^{-1}) with maximum at 3400 cm^{-1} were assigned to the O−H stretching vibration of the residual water, exchangeable OH^-, and defective OH groups with considerable hydrogen bonding. No absorption bands at 1480 and 2800−3000 cm^{-1}, due to the C−H stretching vibration, were observed indicating that surfactant was completely removed upon HCl/EtOH solvent extraction. In the $Zr_{50}Ti_{50}P$ sample, the sharp band (ca. 953 cm^{-1}) appearing in the P−O stretching region was assigned to Ti−O−P or Zr−O−P vibrations. In addition, a very small signal (ca. 1120 cm^{-1}) was also observed in all ZTP solids that was absent in the spectra of $Ti_{100}P$ and $Zr_{100}P$ samples and can be attributed to mixed Ti−O−P−O−Zr framework vibrations. However, the intensity was decreased with increasing zirconium content in ZTP mesoporous solids. Also, a small band appearing at 733 cm^{-1} was due to P−O−P vibrations (see Figure 6).

^{31}P MAS NMR Measurements. The ^{31}P NMR measurements provide useful information regarding the nature of phosphate in ZTP mesoporous solids. The classifications of different possible combinations for tetrahedral phosphorus of various connectivities are listed in Table 3 and abbreviated for easier use. The chemical shifts and the related connectivity of the ^{31}P MAS NMR peaks for the various mesoporous ZTP materials are listed in Table 4. The three resonances can be clearly distinguished in the spectrum of the mesoporous $Zr_{100}P$ material at −6.3, −13.6, and −21.8 ppm from H_3PO_4 (Figure 7) and their position is well matched to those given in zirconium phosphates prepared by a sol−gel process.[23] We have attribute these observed signals to tetrahedral phosphorus of connectivity one $(ZrO)PO_3$, two $(ZrO)_2PO_2$, and three $(ZrO)_3PO$, respectively. Significant numbers of Brønsted acid sites are also available as indicated by the very intense resonance at −21.8 ppm that corresponds to the surface $HOPO_3$ group in α-zirconium phosphate. The sharp peaks with chemical shifts 1.2 and −3.9 ppm were observed for the mesoporous $T_{100}P$ material and assigned to a mixture of tetrahedral phosphorus environments with connectivity three $P(OTi)_3OH$ and four $P(OTi)_4$, respectively. Interestingly, the ^{31}P NMR spectra of mesoporous ZTP solids were somewhat different from those of mesoporous $Ti_{100}P$ and mesoporous $Zr_{100}P$ materials described above. The major change occurring in ^{31}P NMR spectra on altering the Zr/Ti molar ratio was the significant increase both in intensity and in breadth of the field resonance. The gradual increase in chemical shift was also noticed with increasing titanium content in mesoporous ZTP solids that may be related to the progressive condensation of phosphate species in the presence of both titanium and

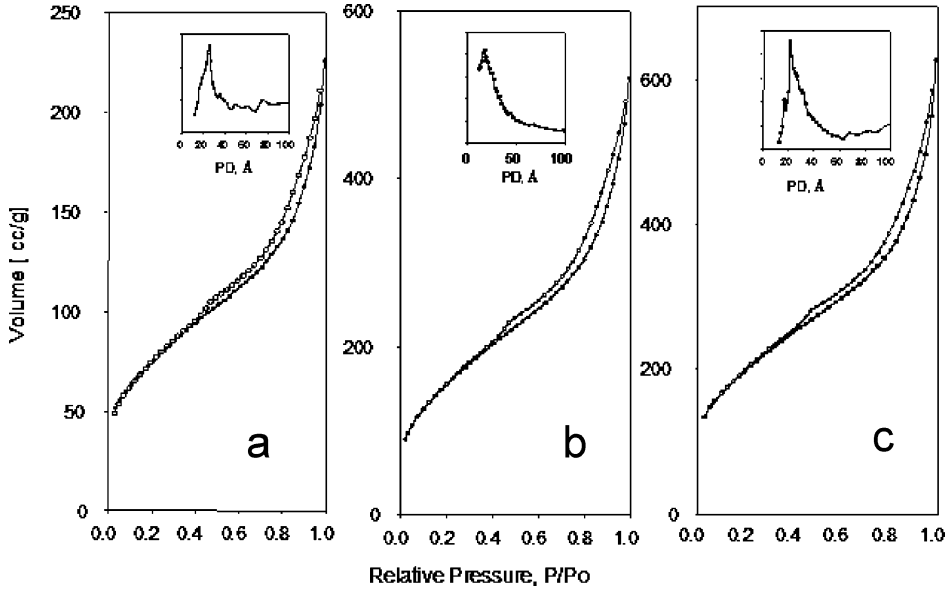

Figure 2. Nitrogen adsorption isotherms and pore size distribution (inset) of mesoporous ZTP materials: (a) $Ti_{100}P$, (b) $Zr_{50}Ti_{50}P$, and (c) $Zr_{100}P$.

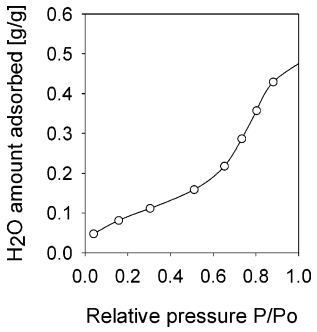

Figure 3. Water adsorption isotherm of representative $Zr_{50}Ti_{50}P$ material.

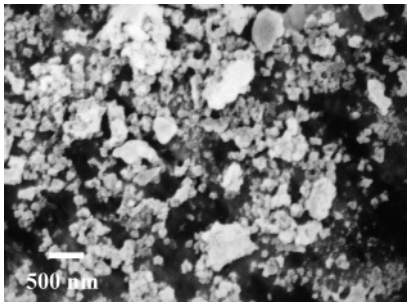

Figure 4. Scanning electron micrograph image of $Zr_{50}Ti_{50}P$ mesoporous material.

zirconium environment. In addition, a very sharp increase in low field signal between −4 to −6 ppm and −12 to −14 ppm with higher titanium containing mesoporous ZTP can also be assigned to several possibilities of phosphate groups linked to both titanium and zirconium with varying connectivity (see classification Table 3). The signals in the range of −27 to −29 ppm indicate the formation of P−O−P bonds and are inline with FTIR results. Similar chemical shifts around −28 to −30 ppm in the tetrahedral phosphorus are also reported for the neutral microporous aluminophosphate materials.[24]

Thermogravimetric Analysis. The TGA/DTA analysis of surfactant free mesoporous $Zr_{50}Ti_{50}P$ material (Figure 8) showed a major weight loss of about 45 wt % in the range 30−100 °C due to water removal. Again, a minimal weight loss observed in the range 100−300 °C was perhaps due to the decomposition of negligible remains of surfactants after extraction, indicating

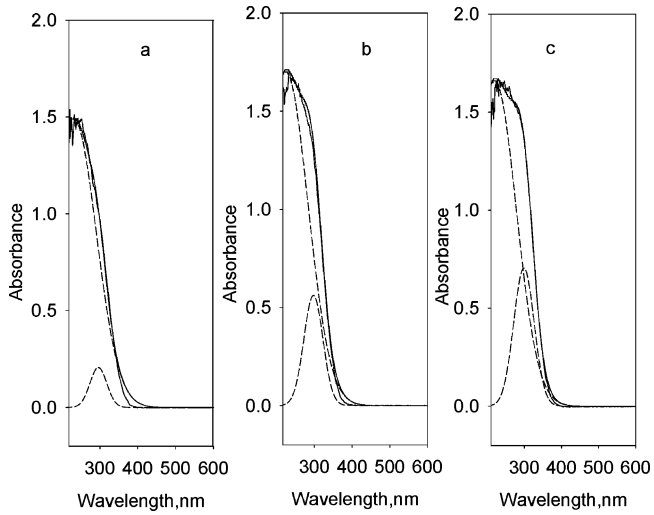

Figure 5. Deconvoluted UV−vis spectra of mesoporous ZTP materials: (a) $Zr_{100}P$, (b) $Zr_{50}Ti_{50}P$, and (c) $Ti_{100}P$ [the details are in Table 2].

TABLE 2: Deconvoluted Details of UV−Visible Spectra of Mesoporous ZTP

	peak 1 (abs 220−235 nm)		peak 2 (abs >290 nm)	
sample entry[a]	intensity, nm	peak area (% total)	intensity, nm	peak area (% total)
$T_{100}P$	234	248 (84.3)	300	46 (15.7)
$Z_{25}T_{75}P$	231	236 (87.7)	298	33 (12.3)
$Z_{50}T_{50}P$	227	228 (90.1)	299	25 (9.9)
$Z_{75}T_{25}P$	224	209 (95.8)	296	9 (4.2)
$Z_{100}P$	221	195 (94.7)	297	11 (5.3)

[a] Key illustrated in Table 1.

that surfactants were almost removed during the solvent extraction process. While in the range of 300−1000 °C the total weight loss measured was only ∼4 wt %. All mesoporous ZTP material showed similar trends.

Ion-Exchange Capacity. The ZTP mesoporous materials also exhibit cation exchange properties due to the defective P−OH groups. Contrary to silanols (Si−OH) where O−H bonding is absolutely covalent, the ionic behavior of the O−H bond in $P-OH^+$ tends to responsible for such cation exchange capacity. The Cl^- form of the mesoporous ZTP samples was potentio-

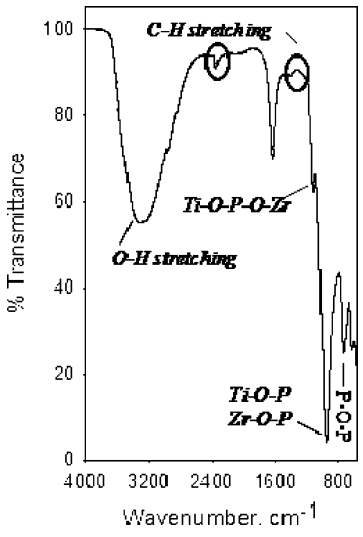

Figure 6. FT-IR spectra of representative $Zr_{50}Ti_{50}P$ mesoporous material.

TABLE 3: Classification Table for the NMR Details

classification for tetrahedral phosphorus	connectivity	abbreviation
only zirconium		
$(ZrO)PO_3$	one	a
$(ZrO)_2PO_2$	two	b
$(ZrO)_3PO$	three	c
$(ZrO)_4P$	four	d
only titanium		
$(TiO)PO_3$;	one	e
$(TiO)_2PO_2$	two	f
$(TiO)_3PO$	three	g
$(TiO)_4P$	four	h
both titanium and zirconium		
$(ZrO)(TiO)PO_2$	two	i
$(ZrO)(TiO)_2PO$	three	j
$(ZrO)_2(TiO)PO$	three	k
$(ZrO)_3(TiO)P$	four	l
$(ZrO)_2(TiO)_2P$	four	m
$(ZrO)(TiO)_3P$	four	n
phosphorus to phosphorus		
P−O−P		o

metrically titrated with a known added amount of aqueous NaOH solution (acid−base titration). The consumed amount of NaOH during the exchange process was quite a bit higher suggesting that the NaOH was consumed not only for exchange from Cl^- to OH^- on the P site but also for exchange from H^+ to Na^+ at the defective $P-O^-$ site. The $Zr_{50}Ti_{50}P$ mesoporous material showed the higher estimated cation-exchange capacity ($\sim$4.73 mmol g^{-1}) compared to mesoporous titanium phosphate and mesoporous zirconium phosphate materials that were 3.08 and 3.99 mmol g^{-1}, respectively.

XANES Measurements. The state of the titanium and the zirconium in the ZTP mesoporous materials was also examined by using the Ti K-egde and Zr K-edge XANES spectra. The photon energies were calibrated by using the edge of pure titanium foil and zirconium foil. For comparison the reference materials TS-1 and TiO_2 anatase for titanium and $ZrSO_4$ for zirconium were also studied. The observed XANES spectra for the reference materials were almost similar to those reported earlier.[25,26] The XANES of the selected ZTP mesoporous materials with varied Zr/Ti molar ratios along with the reference compound are shown in Figure 9. The XANES spectra of the Zr K-edge displayed (Figure 9) showed that general XANES features of the ZTP and reference compound are quite different indicating that the overall structure is very different. A characteristic splitting of the main peak was observed for all mesoporous ZTP solids. While in XANES spectra of Ti K-edge (Figure 9), a small sharp pre-edge peak at 4.968 keV corresponds to 1s−3d excitations involving transitions to the 2t2g and 3eg energy levels.[27,28] The existence of such a peak in all mesoporous ZTP samples revealed that mostly the tetrahedrally coordinated titanium species are present in these materials. In addition, the very weak pre-edge peak at 4.970 keV suggests the mixed coordinate states of titanium in the ZTP materials. Likely most are combinations of four- and five-coordinated Ti species. However, the presence of a fraction of 6-fold coordinated Ti species cannot be excluded because of the adsorption of ambient water. Similar inference was confirmed by UV−vis results. The main absorption peaks in the region 4.970 to 5.025 keV can be assigned to 1s−np dipole transitions. The XANES region also displayed the structure differences between the titanium samples where titanium is surrounded by a different environment and clearly reflects that in the case of mesoporous ZTP materials the −O−P bonding environment is entirely different from the O−Si bonding in reference TS-1 sample.

Thermal and Hydrothermal Stability. In view of the possible catalytic applications, the stability of ZTP mesoporous materials was also examined. Material was extracted with water hydrothermally at ambient temperature for 8 h followed by vacuum-drying and evacuation for 2 h. The lower angle diffraction with slightly reduced intensity in the X-ray diffraction pattern of the material (Figure 10a) confirmed the existence of mesophases. Similarly, the thermal stability was examined by calcining the material at 400 °C for 4 h in air environment and the presence of mesopahse was further confirmed by X-ray diffraction (Figure 10b). The mesopahse was collapse when material was calcined at 550 °C. This result indicates that materials are stable in water and mesoporosity could be retained after treatment even at 400 °C. The plausible mechanism involved in the synthesis of stable ZTP mesoporous materials probably routes via the formation of a phosphate−surfactant ion pair that helps in the subsequent hydrolysis of zirconium and titanium precursors. Once the hydrolysis of both precursors is complete, a sol gel process favors the condensation of Zr and Ti entities with P−OH groups and/or via mixed oxophosphate intermediates that form a hydroxo derivative of zirconium−titanium phosphates in network.

Photocatalysis of Water Splitting for Hydrogen Production. Hydrogen is a clean storable and renewable fuel that does not produce pollutants or green house gases upon combustion. In recent years, photocatalytic splitting of water to hydrogen and oxygen has been regarded as the most promising approach. The UV-light absorption property of titanium phosphate containing mesoporous materials with large surface areas and ion exchange capacity are expected to have utilization as photocatalysts, especially for the hydrogen generation by water decomposition.[12] In the case of ZTP mesoporous materials, the homogeneous pores distribution including the large internal surface area makes such materials accessible to the water molecule and a highly charged structure existing on the surface facilitates the charge separation process essential for the decomposition of water. Herein, we examined the photocatalytic splitting of water for hydrogen production using Pt-loaded ZTP mesoporous materials under UV−vis light irradiation. The experimental setup is shown in Figure 11.

Table 5 lists some textural properties of the Pt loaded mesoporous ZTP catalysts. The surface area of the Pt was determined by using carbon monoxide (CO) adsorption carried

TABLE 4: Description of the Chemical Shifts and Possible Connectivity Type in Mesoporous ZTP Materials

	sample description: chemical shift, ppm) (possible connectivity type[a])				
connectivity	Ti_{100}	$Z_{25}Ti_{75}$	$Z_{50}Ti_{50}$	$Z_{75}Ti_{25}$	Z_{100}
one	nd (e)	−4.2 (a)	−5.1 (a)	−6.1 (a)	−6.3 (a)
two	nd (f)	−11.4 (b, i)	−12.5 (b, i)	−13.1 (b, i)	−13.6 (b)
three	1.2 (g)	−18.1 (c, j, k)	−21.6 (c, j, k)	−21.7 (c, j, k)	−21.8 (c)
four	−3.9 (h)	nd (d, l, m, n)	nd (d, l, m, n)	nd (d, l, m, n)	nd (d)
P−O−P type	−27.9 (o)	−26.3 (o)	−27.6 (o)	−27.5 (o)	−27.6 (o)

[a] Table 3 gives the key for the connectivity type.

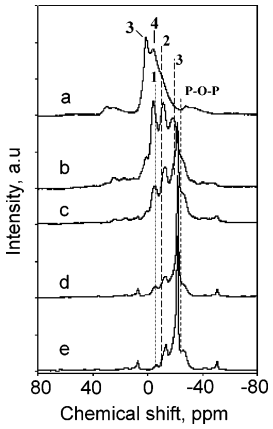

Figure 7. ^{31}P MAS NMR spectra of mesoporous ZTP materials: (a) $Ti_{100}P$, (b) $Zr_{25}Ti_{75}P$, (c) $Zr_{50}Ti_{50}P$, (d) $Zr_{75}Ti_{25}P$, and (e) $Zr_{100}P$.

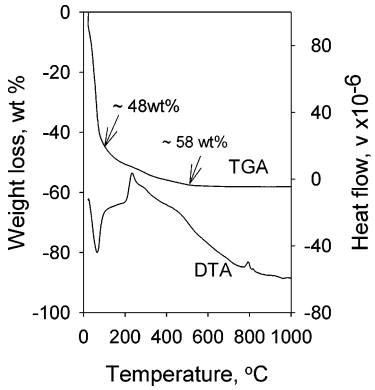

Figure 8. TGA/DTA analysis of representative $Zr_{50}Ti_{50}P$ mesoporous material.

out on the sample prereduced at 300 °C. The metallic surface areas of the Pt were calculated from the quantity of CO chemisorbed on the surface assuming that CO atoms are stoichiometrically adsorbed on the Pt atom. The Pt dispersion and Pt particle size were also determined and are listed in Table 5.

As expected, compared to mesoporous titanium phosphate (ca. 0.91 μmol/h·g^{-1} cat), comparatively large amount (~6-fold; ca. 5.35 μmol/h·g^{-1} cat) of H_2 was produced over the mesoporous zirconium phosphate. Also, the H_2 production was lowered when conventional mesoporous TiO_2 was used under similar reaction conditions (Figure 12). Surprisingly, the mixed mesoporous zirconium titanium phosphates (ZTP) with a varied range of compositions showed an enhanced photoactivity for H_2 production. H_2 evolution was ~9-fold higher (ca. 5.51 μmol/h·g^{-1} cat) when catalyst was reduced properly under hydrogen flow (Figure 13). One possibility is that the reduction of Pt was not completed when the catalyst was reduced in situ photocatalytically (ca. 0.51 μmol/h·g^{-1} cat). Also, the higher Pt loading resulted in enhanced H_2 evolution. The catalysts were least active without Pt deposition (ca. 0.25 μmol/h·g^{-1} cat). Even at

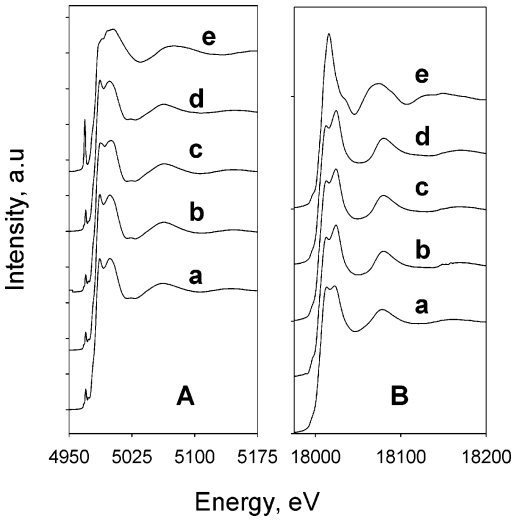

Figure 9. XANES spectra of ZTP mesoporous materials: (A) Ti K-edge [(a) $Ti_{100}P$, (b) $Zr_{25}Ti_{75}P$, (c) $Zr_{50}Ti_{50}P$, (d) $Zr_{75}Ti_{25}P$, and (e) reference TS-1] and (B) Zr K-edge [(a) $Zr_{100}P$, (b)$Zr_{75}Ti_{25}P$, (c) $Zr_{50}Ti_{50}P$, (d) $Zr_{25}Ti_{75}P$, and (e) reference $ZrSO_4$].

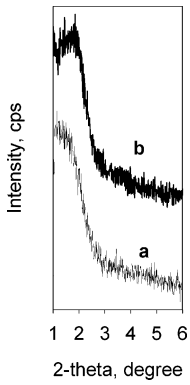

Figure 10. Thermal and hydrothermal stability of $Zr_{50}Ti_{50}P$ mesoporous material (a) after calcinations at 400 °C and (b) after extraction with hot water.

0.2 wt % of Pt loading the hydrogen production was significant (ca. 5.51 μmol/h·g^{-1} cat) and further increased by ~1.6-fold (ca. 8.86 μmol/h·g^{-1} cat) for the catalyst with 1 wt % of Pt loadings (Figure 14). This increase may be due to the increased number of active species on the catalyst surface.

Hydrogen production as a function of Zr addition to the mesoporous titanium phosphate catalysts showed that the H_2 production rate was gradually increased on addition of Zr and maximum H_2 evolution of ca. 8.86 μmol/h·g^{-1} cat was observed for the $Z_{50}T_{50}P$ material (Figure 15). This describes the synergetic effect of zirconium on titanium in ZTP mesoporous materials.

Further, without sodium carbonate the H_2 production rate was ca. 0.69 μmol/h·g^{-1} cat, while without catalyst only ca. 0.05 μmol/h·g^{-1} cat hydrogen was produced. This indicates that the use of sodium carbonate as pH adjuster was essential and

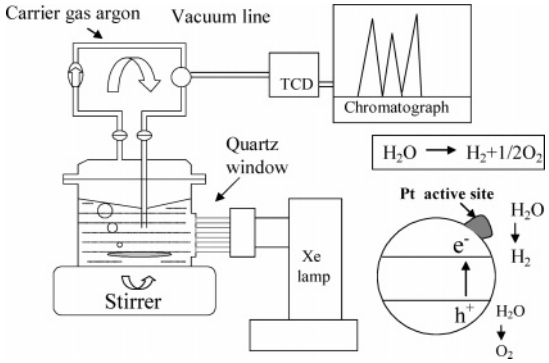

Figure 11. Schematic diagram of the setup of the reactor for photoinduced water splitting for hydrogen production.

TABLE 5. Important Textural Properties of 1% Pt/ZTP Catalysts

1% Pt/ sample type[a]	CO chemically adsd, mol/g × 10^{-6}	Pt surface. area, m^2/g	Pt particle size, Å	Pt dispersion (total), %
$T_{100}P$	1.20	0.111	209.5	2.34
$Z_5T_{95}P$	1.88	0.174	134.0	3.66
$Z_{10}T_{90}P$	2.11	0.196	119.0	4.12
$Z_{20}T_{80}P$	2.14	0.199	117.3	4.18
$Z_{25}T_{75}P$	3.08	0.286	81.6	6.01
$Z_{50}T_{50}P$	4.37	0.405	57.5	8.53
$Z_{100}P$	7.43	0.689	33.8	14.5

[a] 1% Pt = 5.126 × 10^{-6} mol/g.

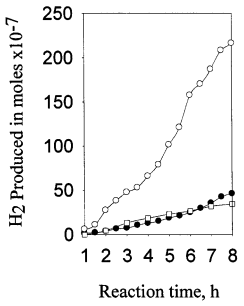

Figure 12. Hydrogen production rates as a function of reaction time on (●) 1% $Pt/TiPO_4$, (○) 1% $Pt/ZrPO_4$, and (□) 1% Pt/TiO_2 mesoporous materials.

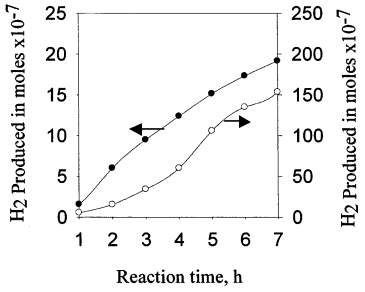

Figure 13. Hydrogen production rates as a function of reaction time on 0.2% $Pt/Zr_{50}Ti_{50}P$ mesoporous material [(●) photoreduced, rt, 24 h; and (○) H_2 reduced, 300 °C, 3h].

significant for hydrogen generation and also provides the stability of the photocatalytic reaction system. The formation of a considerable amount of oxygen during the reaction was also observed. However, the determination of the actual amount of oxygen formed in the photoinduced reaction was rather difficult due to the problems in apparatus handling. Similar to the mesoporous titanium phosphate materials,[2] the energy gaps in the mesoporous ZTP solids were estimated to be ca. 3.8 eV, which is larger than that reported for TiO_2 (ca. 3.0 eV). This is

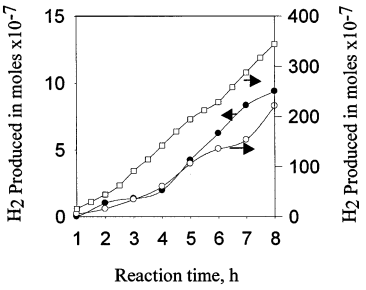

Figure 14. Effect of Pt loading on the hydrogen production rates as a function of reaction time on the (●) $Zr_{50}Ti_{50}P$, (○) 0.2% $Pt/Zr_{50}Ti_{50}P$, and (□) 1% $Pt/Zr_{50}Ti_{50}P$ mesoporous materials.

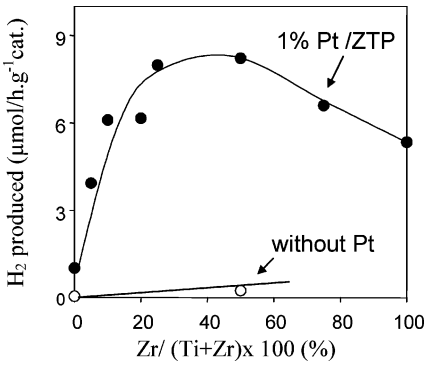

Figure 15. Hydrogen production rates as a function of zirconium addition in ZTP mesoporous materials.

also probably the reason that ZTP mesoporous material showed improved catalytic activity in photoinduced water splitting for the hydrogen production.

4. Conclusions

We have successfully demonstrated the synthesis of mesoporous mixed zirconium−titanium phosphate (ZTP) materials using cationic surfactant at room temperature. Materials were relatively less ordered mesophases compared to its earlier reported silica analogues and revealed that either pore walls of the materials are amorphous or a lack of correspondence between the structure of adjacent pores. This also suggests that materials have a small crystalline domain size and the degree of ordering was limited in the channel packing. Ti K-edge XANES suggested the mixed coordinate states of titanium and zirconium in the ZTP mesoporous materials. Likely most are combinations of four- and five-coordinated Ti species along with a fraction of 6-fold coordinated Ti moieties that was confirmed by UV−vis and a high level adsorption of ambient water at low P/P_o.The results also confirmed that the charge can be generated and exchangeable sites are available in the materials. Also, the changes in phosphorus connectivity with varied Zr/Ti ratio indicate the synergic effect of zirconium on titanium in ZTP mesoporous solids. Finally, the results of photocatalytic decomposition of water for the hydrogen generation evidently suggest that mesoporous ZTP materials are possible candidates of photocatalysts for hydrogen production. Detailed photocatalytic experiments are currently underway and will be the subject of a future contribution on an attempt to construct a photosynthetic system to replace exhausting fossil fuels by using solar energy.

Acknowledgment. The X-ray absorption experiments were performed under the approval of the Photon Factory Program Advisory Committee (Proposal No. 2001G097).

References and Notes

(1) Pastor, P. O.; Torres, P. M.; Castellon, E. R.; Lopez, A. J. *Chem. Mater*. **1996**, *8*, 1758.

(2) Clearfield, A. *Chem. Mater*. **1998**, *10*, 2801.

(3) Wilson, S. T.; Lok, B. M.; Messina, C. A.; Cannon T. R.; Flanigan, E. M. *J. Am. Chem. Soc*. **1982**, *104*, 1146.

(4) Kimura, T.; Sugahara, Y.; Kuroda, K. *Microporous Mesoporous Mater*. **1998**, *22*, 115.

(5) Kapoor, M. P.; Raj, A. *Appl. Catal.* **2000**, *203*, 311.

(6) Pacheco, G.; Zhao, E.; Garcia, A.; Sklyarov A.; Fripiat, J. J. *Chem. Commun.* **1997**, 491.

(7) Antoneli D. M.; Ying, J. Y. *Angew. Chem., Int. Ed. Engl*, **1995**, *34*, 2014.

(8) Abe, T.; Taguchi A.; Iwamoto, M. *Chem. Mater*. **1995**, *7*, 1429.

(9) Jimenez, J. J.; Torres, P. M.; Pastor, P. O.; Castellon, E. R.; Lopez, A. J.; Jones D. J.; Roziere, J. *Adv. Mater*. **1998**, *10*, 812.

(10) Jones, D. J.; Aptel, G.; Brandhorst M. *J. Mater. Chem.* **2000**, *10*, 1957.

(11) Sun, Y.; Afanasiev, P.; Vrinat M.; Coudurier, G. *J. Mater. Chem.* **2000**, *10*, 2320.

(12) Bhaumik A.; Inagaki, S. *J. Am. Chem. Soc.* **2001**, *123*, 691.

(13) Castellon, E. R.; Jimenez, J. J.; Lopez, A. J.; Torres, P. M.; Barrado, J. R. R.; Jones, D. J.; Roziere, J. *Solid State Ionics* **1999**, *125*, 407.

(14) Hasan, S. S. M.; Marei, S. A.; Badr, I. H.; Arida, H. A. *Anal. Chim. Acta* **2001**, *427*, 21.

(15) Prior to the in situ photoreduction, water (∼14 Torr) was first adsorbed for 2 h on the evacuated sample followed by the methanol vapors (∼18 Torr) for 2 h. Then the sample was photoreduction under UV radiation with a Hg lamp for 24 h.

(16) Yang, P.; Zaho, D.; Margolese, D. I.; Chmelka, B. F.; Stucky, G. D. *Nature* **1998**, *396*, 152.

(17) Kresge, C. T.; Leonowicz Roth, W. J.; Vartuli, J. C.; Beck, J. S. *Nature* **1992**, *359*, 710.

(18) Sono, T.; Fukuta, S.; Wang, Z. B.; Soga, K. *Proc. 12th IZC Baltimore* **1998**, *1*, 301.

(19) Wang, Z. B.; Ikeya, H.; Sono T.; Soga, K. *Proc. 12th IZC Baltimore* **1998**, *1*, 293.

(20) Inagaki, S.; Fukushima, Y. *Microporous Mesoporous Mater*. **1998**, *21*, 667.

(21) Ribeiro-Carrott, M. M. L.; Candeias, A. J. E.; Carrott, P. J. M.; Unger, K. K. *Langmuir* **1999**, *15*, 8895.

(22) Kosuge, K.; Sing, P. S. *J. Phys. Chem*. **1999**, *103*, 3563.

(23) Benhamza, H.; Barboux, P.; Bouhaouss, A.; Josien A.; Livage, J. *J. Mater. Chem.* **1991**, *1*, 681.

(24) Blackwell, C. S.; Patton, R. L. *J. Phys. Chem.* **1984**, *88*, 6135.

(25) Salama, T. M.; Tanaka, T.; Yamaguchi, T.; Tanabe, K. *Surf. Sci. Lett.* **1990**, *227*, L100.

(26) Thomas, J. M.; Sankar, G. *J. Synchrotron Radiat.* **2001**, *8*, 55.

(27) Poumellec, B.; Marucco J. F.; Touzelin, B. *Phys. Rev. B* **1987**, *35*, 2284.

(28) Grunes, L. A. *Phys. Rev. B* **1983**, *27*, 2111.